Identifying and Mitigating Model Failures through Few-shot CLIP-aided Diffusion Generation

Anonymous authors
Paper under double-blind review

Abstract

Deep learning models encounter unexpected failures, especially when dealing with challenging sub-populations. One common reason for these failures is features that the data may be spuriously correlated with. To better understand these failure modes, human-interpretable descriptions are crucial, which is expensive. In this study, we propose an end-to-end framework that utilizes the capabilities of large language models (ChatGPT) and vision-language deep models (CLIP) to generate text descriptions of failure modes associated with spurious correlations (e.g., rarely seen backgrounds) without human-in-the-loop intervention. These descriptions can be used to generate synthetic data using generative models, such as diffusion models. The model can now use this generated data to learn from its weaknesses and enhance its performance. Our approach serves as a broad solution, promising progress in comprehending model failure modes and strengthening deep learning models automatically across a wide range of failure scenarios (e.g., backgrounds, colors) in a few-shot manner. Our experiments have shown remarkable **improvements in accuracy ($\sim$ 21%)** on hard sub-populations (particularly for wrong background association) across 30 different models, such as ResNets, EfficientNets, DenseNets, Vision Transformer (ViT), SwAVs, MoCos and DINOs on various datasets such as ImageNet-1000, and CIFAR-100, iNaturalist-2018.

1 Introduction

The quality of training data directly impacts the performance and robustness of machine learning models. Despite careful curation of training data, models can still exhibit failure modes where their performance deteriorates in specific sub-populations of data, leading to misclassifications or inaccurate predictions Jiang et al. (2018); Arpit et al. (2017). The failure modes of deep networks can arise from various factors, such as noisy labels Sukhbaatar et al. (2014); Jiang et al. (2018); Reed et al. (2015), multi-labels Zhang et al. (2018b), and spurious correlations Zhou et al. (2020), particularly when it comes to distinguishing between objects and their backgrounds Kattakinda & Feizi (2021); Xiao et al. (2021). (See Figure 7 in appendix for examples of these failures.)

Similar to how humans use image backgrounds as cues for object recognition, studies have shown that machine learning models also rely on backgrounds when making decisions. In some cases, models may prioritize backgrounds to the point of overlooking important object features for classification Zhang et al. (2007); Ribeiro et al. (2016); Sagawa et al. (2020).

Various strategies have been attempted to mitigate failure modes caused by spurious background associations, but many are insufficient in addressing the entirety of the problem. Some methods involve human-in-the-loop interventions Mitchell et al. (2021); Santurkar et al. (2021), which are both labor-intensive and challenging to scale for large operations. Furthermore, many of these approaches specifically target only one spurious correlation, such as background, and may not be readily applicable to other correlations like colors, thus neglecting a comprehensive spectrum of potential failures Barbu et al. (2019); Hendrycks et al. (2021a); Hendrycks & Dietterich (2019); Hendrycks et al. (2021b); Kattakinda & Feizi (2021). Additionally, certain existing works lack clear descriptions of model failures in a human-understandable manner, posing challenges in terms of interpretability and validation.

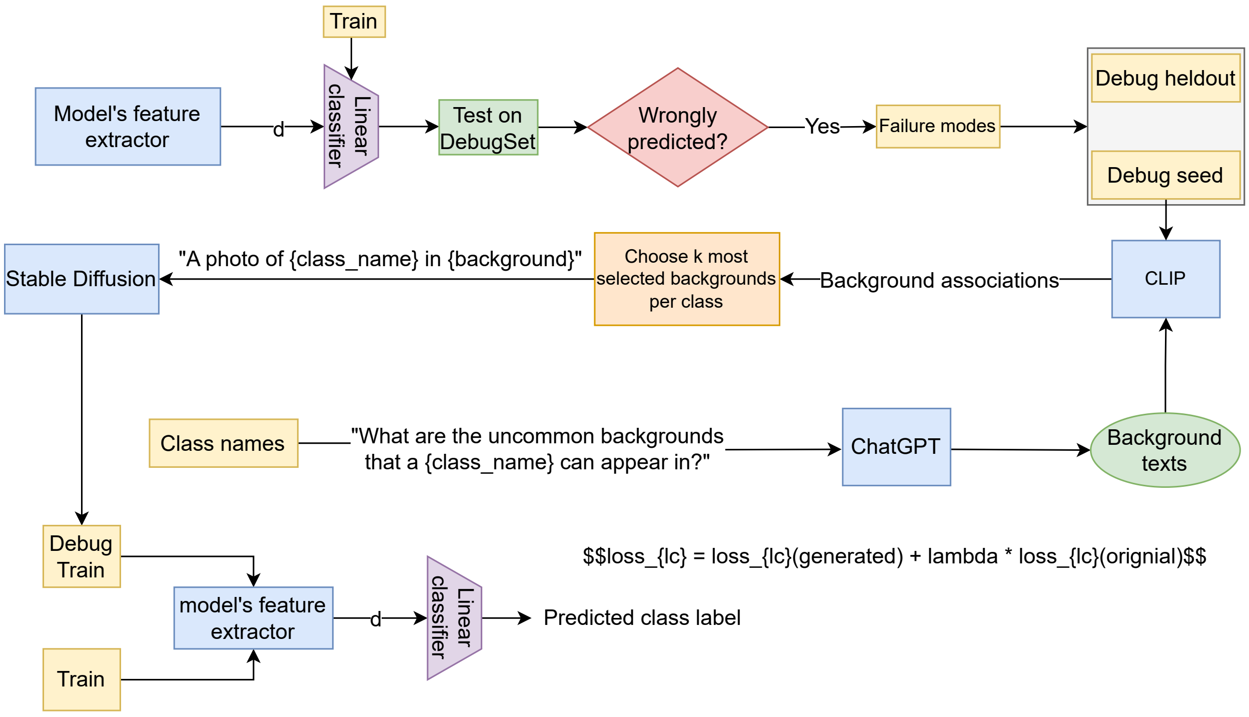
Train
Model's feature extractor
d
Linear classifier
Test on DebugSet
Wrongly predicted?
Yes
Failure modes
Debug heldout
Debug seed
CLIP
Background associations
Choose k most selected backgrounds per class
"A photo of {class_name} in {background}"
Stable Diffusion
Class names
"What are the uncommon backgrounds that a {class_name} can appear in?"
ChatGPT
Background texts
Debug Train
Train
model's feature extractor
d
Linear classifier
Predicted class label
$$loss_{lc} = loss_{lc}(generated) + lambda * loss_{lc}(orignial)$$

Figure 1: A summary of our approach applied to background spurious correlations: For a model based on the wrongly predicted debug samples (failure samples), we form two sets - ***DebugSeed*** and ***DebugHeldout***. We use the ***DebugSeed*** set to address the model's failures by inputting them to CLIP Radford et al. (2021), along with a set of backgrounds obtained from ChatGPT where objects are less likely to occur with the data. We then obtain a set of backgrounds and remove redundancies, and generate synthetic data by inputting the prompt "A photo of {class_name} {background}" to Stable Diffusion Rombach et al. (2021). With this synthetic data that precisely captures the model's failure modes related to backgrounds, we can now refine the model's predictions on other test data by training a very low-cost linear head on top of our model, which assigns different weights to the original data and the generated data.

In conjunction with research on identifying failure modes, there are various **refinement** approaches aimed at leveraging these failure modes to improve the accuracy of machine learning models. These strategies involve actions such as generating additional datasets containing failure samples to assist the model in learning robust features Xiao et al. (2021); Singla et al. (2024) or adjusting the model's parameters to integrate information derived from identified failure modes Rame et al. (2022). However, these studies often lack easily understandable descriptions of failure modes for human interpretation, posing challenges in assessing their validity. Furthermore, these refinement approaches are typically not automated.

2 Our contribution

This research leverages recent generative models, large language models, and CLIP to introduce an automated framework addressing failure modes (spurious correlations) in diverse task-specific deep learning models. The framework, outlined in Figure 1, answers critical questions such as identifying and rectifying spurious associations leading to model failure, utilizing these failure modes to refine models, exploring patterns in failure modes across a model group, and using a single set of auxiliary data to improve a subgroup of models simultaneously.

To summarize, our approach initially identifies all model failures on a specific subset, denoted as ***DebugSet***, which is a part of the validation set. We then pinpoint spurious correlations, such as background associations, for each dataset class by querying ChatGPT with "What are the uncommon backgrounds that a class_name can appear in?" and remove redundancies after obtaining uncommon backgrounds for all classes. Subsequently, a zero-shot classification using CLIP identifies the background for each failure among all the uncommon backgrounds. To enhance model performance, we generate ***k*** artificial images with prompts like "[class_name] in [background_name]" and incorporate this supplementary data into the original_train_set. In the second phase, we demonstrate that models with similar architectures exhibit analogous failures, allowing efficient troubleshooting of a group of models using a single set of generated auxiliary data. This approach proves both time and memory-efficient. The results of our experiments, detailed in section 5, underscore the effectiveness of this straightforward method in achieving interpretability and refinement goals.

Our paper presents several contributions to model failure analysis and refinement. These contributions include, but are not limited to, the following:

- **Generalizability**: Introducing an automatic end-to-end framework that interprets and rectifies failures arising from specific spurious associations, such as incorrect background, color, and size correlations, which can contribute to any model inaccuracies.
- **Failure Inspection**: Identification of spurious associations(section 5.2.1), and exploring common patterns in failure modes among individual models with same architectures (section 5.2.2) in an interpretable manner .
- **Failure Mitigation**: Improving the performance of individual models on challenging sub-populations (5.3.1), and boosting the performance of a subset of models by employing a unified set of auxiliary data, leveraging shared failures to enhance efficiency in both time and memory usage (section 5.3.2).
- **Collective Failure Mitigation**: Refinement of a subset of models' performance through a unified set of auxiliary data owing to their shared failures, which saves time and memory. **To the best of our knowledge, this work represents the first effort to collectively address failures within a subgroup of models simultaneously. (section 5.3.2).**

3 Related work

3.1 Failure mode detection

Numerous studies have been conducted to detect failure modes in machine learning models. Some involve human-in-the-loop methods, where failure examples are reviewed to identify common patterns Mitchell et al. (2021); Santurkar et al. (2021). Others adopt automated approaches by introducing frameworks that effectively capture model failures Chung et al. (2019); Singla et al. (2021); Nushi et al. (2018); Singla & Feizi (2022); Wong et al. (2021); Wu et al. (2019); Zhang et al. (2018a); Jain et al. (2023). For instance, Chung et al. (2019) employs a technique that slices the validation data to isolate sections where the model performs poorly. Singla et al. (2021) identifies visual attributes that lead to inadequate performance when present or absent. Jain et al. (2023) identifies and represents model failures as directions in the latent space, and Eyuboglu et al. (2022) proposes an evaluation framework to systematically compare (slice discovery method) SDMs across diverse slice settings by generating captions for hard sub-populations. Distinguishing itself from existing methodologies, our approach provides enhanced generality by **permitting the explicit selection of the spurious correlation targeted for mitigation, targeted data collection, giving interpretable descriptions for failures, and being an automatic approach**. For instance, although the approach presented by Kattakinda et al. Kattakinda et al. (2022) effectively tackles spurious correlations tied to foreground and background features by learning disentangled representations, it encounters difficulties when confronted with a broader spectrum of spurious correlations, e.g., color. This is due to the inherent challenge of learning disentangled representations for many spurious correlations in isolation from the foreground object.

3.2 Mitigation of Hard Subpopulations and Interpretability of Models

Several methodologies leverage extracted failure modes to enhance the performance of deep learning models. Singla et al. (2024) introduce a framework that identifies visually similar images to model failures and incorporates them as new data for refinement of various models. Kattakinda et al. (2022) focus on learning invariant features for foreground and background by penalizing the mutual information between the features and background/foreground labels. This approach contributes to robust model training, particularly by addressing issues related to spurious correlations.

In data generation, Bansal & Grover (2023), and Wiles et al. (2022) use generated data to diversify training datasets. However, it's essential to note that their methods do not specifically target failure modes like spurious correlations. They rely on class names and general captions for generating auxiliary data, which may not be tailored to address specific failure modes.

Moreover, Wiles et al. (2022) propose a bug discovery approach using off-the-shelf image generation and captioning, contributing to the interpretability of model predictions. On the other hand, Jain et al. (2023) leverage Support Vector Machines (SVMs) to distill model failures as directions in latent space, focusing on latent representations of model failures.

Compared to existing methodologies that address failure modes on specific datasets, our framework introduces two noteworthy contributions. Firstly, **it achieves enhanced model performance with significantly fewer generated examples (5 for each failure)**. Secondly, **our experiments extend to collective refinement, demonstrating the ability to improve a subset of model failures by generating a single auxiliary artificial dataset based on only one model's failures**. This is particularly valuable given our observation that models within the same categories exhibit similar failures, a phenomenon also noted in Wiles et al. (2022).

Moreover, our approach is efficient, eliminating the necessity for complete model retraining or fine-tuning. We exclusively focus on retraining the linear head for classification, streamlining the failure mode mitigation process.

3.3 Synthetic data as data augmentation

Numerous studies leverage the generative capabilities of diffusion and GAN models to produce synthetic data, enhancing training datasets for better accuracy in downstream tasks. For example, in work by Hong et al. (2023), a classifier is trained using consistency rules on unlabeled data generated from unconditional GANs, improving image classification. Zhou et al. (2023) employ the Stable Diffusion model to generate diverse and high-quality training data for image classification efficiently. The theoretical aspect of using synthetic data and its stability bound is explored by Zheng et al. (2023), offering insights into improved learning rates achievable with generative data augmentation, especially in small training set scenarios. Ye-Bin et al. (2023) address the data imbalance problem by generating synthetic data. Additionally, Luzi et al. (2022) introduces varied, nonidentical images through a partial reverse diffusion process, serving as a data augmentation method to enrich training datasets. Various image editing methods Meng et al. (2021); Kawar et al. (2023); Zhang et al. (2023); Brooks et al. (2023); Mokady et al. (2023); Koohpayegani et al. (2023) can also be considered for synthetic data generation to enhance training datasets. Our method uses the targeted generation of synthetic data for hard subpopulations as data augmentation to address the problem of spurious correlations.

4 Main method

4.1 Failure-mode detection

A common reason for accuracy drops during inference is the model's learned spurious correlations from training. For example, Associating objects with backgrounds, a spurious correlation can hinder the model's ability to learn about objects themselves. This challenge arises when the model encounters objects in unfamiliar backgrounds during testing, notably in computer vision tasks where backgrounds define object context. To tackle this, introducing the model to a range of scenarios that address the particular failure mode (such as color or background associations) we aim to mitigate can improve its ability to identify objects in different contexts and avoid correlating the objects and their changeable features (e.g., color) or contexts (e.g., background).

Initially designed to rectify wrong background associations, our framework can be extended to address various spurious correlations. We showcase its applicability by presenting results for color spurious associations in 5.

To address and rectify failures attributed to backgrounds, we utilize the feature extractor for each model on the datasets, generating a feature vector for each data point. The subsequent linear head atop this feature extractor executes the classification task. Instances where the model makes incorrect predictions form a set termed the ***DebugSet***, which serves as a tool for identifying and resolving failure modes, comprising all examples where the model fails. While these failures may stem from various factors, our experiments underscore the significance of mitigating incorrect background associations, as they significantly improve the performance of all models.

4.2 Failure-mode textualization

Vision-language models are popular as they can provide a more comprehensive understanding of complex phenomena by combining information from different modalities like text, images, and audio, enabling them to interpret data in a more human-readable form Lu et al. (2019); Chen et al. (2018); Mithun et al. (2020).

Understanding failure modes is critical for validating proposed refinement methods. By identifying the causes of failure, we can improve our models and refine our data collection methods. For each class_name in our dataset, we first prompt ChatGPT, "What are the uncommon backgrounds that a class_name can appear in?" filter out the redundant suggested backgrounds and keep the 10 suggested uncommon backgrounds for each class. Some examples can be seen in Table 1. Then, we use CLIP Radford et al. (2021) to interpret failure modes by splitting the failures from the ***DebugSet*** into two sets called ***DebugSeed*** and ***DebugHeldout***. We then perform zero-shot classification by passing ***DebugSeed*** along the set of uncommon backgrounds proposed by ChatGPT to a CLIP model, so for each data point, CLIP will opt for the background that is more likely to be the actual background of the object shown in the image. For each data class, we then pinpoint the ***k*** most frequently selected backgrounds by CLIP, which the model failed to classify. Our experiments, as depicted in Figure 5, indicate that the optimal value for k, which is both small and practical, is 3. While increasing the value of ***k*** may enhance final results, the marginal improvement is negligible compared to the cost and time associated with generating additional synthetic data. This will provide valuable insights into how a model may fail when confronted with a particular selected spurious association.

Class name	Uncommon backgrounds
Sea lion	Desert, Rain forests, Urban Areas, Polar Ice Caps, Caves, Grasslands, Volcanic Areas
Siberian Husky	Jungle Canopies, In the Sky, Caves, Underwater, Indoor Spaces, Marshlands, Tropical Rainforests
croquet ball	Mountain Peaks, Busy Streets, Frozen Lakes, Underneath Building Foundations, Subway Tunnels, in a restaurant
lipstick, lip rouge	Gyms and Fitness Centers, Swimming Pools, Medical Facilities, Construction Sites, Sports Events, Military Training

Table 1: Examples of suggested uncommon backgrounds for a class of data by ChatGPT

4.3 Generating synthetic data

By leveraging CLIP's detected backgrounds of failures, we can interpret them and use them to refine models. For instance, in the case of the ImageNet class "tench," errors predominantly occur when the fish is held by a person's hand, a scenario rarely encountered during training. To address this, a generative model like Stable

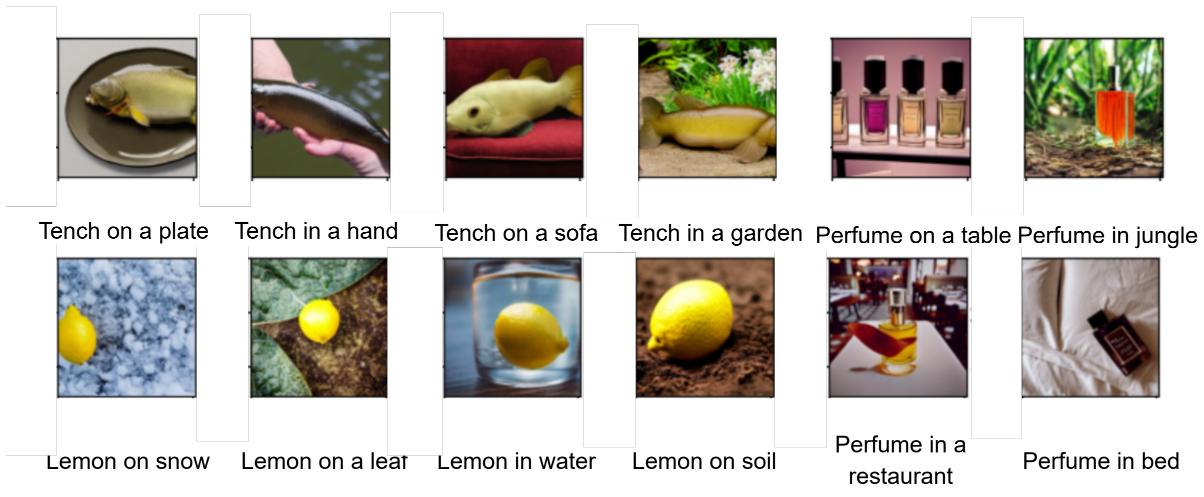

Figure 2: Examples of generated data by Stable Diffusion

Diffusion Rombach et al. (2021) can create images that familiarize the model with diverse object contexts. We generate data for the "tench" class by inputting the prompt "tench in hand" to the Stable Diffusion. Examples of such generated data are presented in Figure 2

4.4 Retraining the linear head

After collecting the additional synthetic data for the failed scenarios, which we call ***DebugTrain***, we can use it along with our original_train_set to refine our models. To achieve this, we only need to train a linear head on top of the model's feature extractor for classification purposes, not the whole model. We must note that we assign different weights to the data points from the original_train_set and the ***DebugTrain*** set in our linear head training loss 1. This parameter is called ***lambda***, and in our experiments shown in 5, we report its effect on the overall performance of the model. By incorporating the additional ***DebugTrain*** data and carefully tuning the ***lambda*** parameter, we can potentially improve the performance of our models.

$$L_{cl} = L_{cl}(Original\_train\_set) + \lambda * L_{cl}(DebugTrain) \tag{1}$$

5 Experiments

5.1 Setting

We conducted experiments on 40 pretrained models, including ResNets He et al. (2016), EfficientNets Tan & Le (2019), DenseNets Huang et al. (2017), Vision Transformer (ViT) Dosovitskiy et al. (2021), SwAVs Caron et al. (2020), MoCos He et al. (2019), DINOs Caron et al. (2021), and CLIPs Radford et al. (2021). The complete list of models is available in Table 6 in the appendix. For brevity, we present results for DINO and ResNet models, and additional experiments for other models are provided in Appendix **??**.

For each dataset, we input the data into the models to obtain extracted features. A linear head was then trained on top of these features. In the case of ImageNet, the linear head was trained using 30 data points per class from the overall 30,000 training images. We designated 30,000 images from the ImageNet validation set as our ***DebugSet*** (30 per class), with the remaining 20,000 samples used for testing. The images had a resolution of 224×224, and the task was ImageNet classification.

The hyperparameters and other settings are detailed in Table 5 in the appendix.

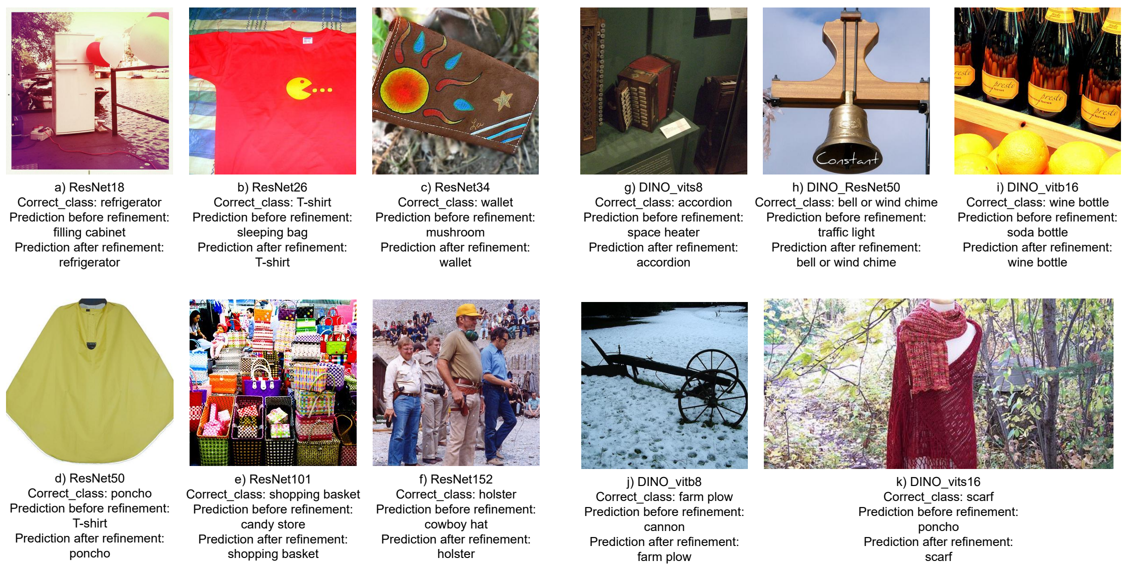
a) ResNet18
Correct_class: refrigerator
Prediction before refinement:
filling cabinet
Prediction after refinement:
refrigerator
b) ResNet26
Correct_class: T-shirt
Prediction before refinement:
sleeping bag
Prediction after refinement:
T-shirt
c) ResNet34
Correct_class: wallet
Prediction before refinement:
mushroom
Prediction after refinement:
wallet
g) DINO_vits8
Correct_class: accordion
Prediction before refinement:
space heater
Prediction after refinement:
accordion
h) DINO_ResNet50
Correct_class: bell or wind chime
Prediction before refinement:
traffic light
Prediction after refinement:
bell or wind chime
i) DINO_vitb16
Correct_class: wine bottle
Prediction before refinement:
soda bottle
Prediction after refinement:
wine bottle
d) ResNet50
Correct_class: poncho
Prediction before refinement:
T-shirt
Prediction after refinement:
poncho
e) ResNet101
Correct_class: shopping basket
Prediction before refinement:
candy store
Prediction after refinement:
shopping basket
f) ResNet152
Correct_class: holster
Prediction before refinement:
cowboy hat
Prediction after refinement:
holster
j) DINO_vitb8
Correct_class: farm plow
Prediction before refinement:
cannon
Prediction after refinement:
farm plow
k) DINO_vits16
Correct_class: scarf
Prediction before refinement:
poncho
Prediction after refinement:
scarf

Figure 3: Some examples of failure modes of ResNets and DINOs

To address detected failures in the ***DebugSet***, we split them in half. The first half, ***DebugSeed***, was used for refinement. Uncommon backgrounds were generated using ChatGPT 3.5. The CLIP model used for selecting backgrounds for data points was ViT-B/32 CLIP. For synthetic data generation, we utilized Stable Diffusion V1-5 imported from the diffusers package von Platen et al..

5.2 Failure inspection

The initial stage of our framework involves analyzing how various models fail to classify objects in different datasets. To accomplish this, we use the CLIP model to identify backgrounds on which models struggle to classify objects. This results in captions that describe failures related to rare backgrounds. In the following stage, we examine these identified failures and explore how the generated captions help us to recover from them. We investigate results for both **individual and collective failure inspection**.

5.2.1 Individual Failure Inspection

In Figure 3, we show some instances where ResNet and DINO models have failed and see that these failures are due to wrong background association. In this Figure, the six images on the left (a-f) are examples of Resnets' failures, and the five images on the right (g-k) are failure modes' of DINO models. For example, image ***c*** shows *"a wallet in jungle"*, which can be regarded as an uncommon background for this object. As a result, the ResNet34 model is unable to classify it accurately and instead predicts a *"mushroom"* which is more likely to be found *"in jungle"*, especially under a plant, despite having no resemblance to the actual object in the image. Similarly, image ***h*** illustrates *"a bell or wind chime in sky"*, which is uncommon since *"bell"* is more likely to be seen with other backgrounds such as *"a door, a building or a wall"*. Therefore, the DINO_reset50 model mispredicts as *"traffic light"* because *"traffic light"* is more common to be seen *"in a sky background"*.

In general, our approach is capable of addressing failure scenarios originating from uncommon backgrounds of objects or any other spurious correlation (We provide another instance demonstrating how our framework can be applied to analyze another type of spurious correlation, such as color, in 5.3.2). Analyzing the relevant backgrounds allows us to readily understand the cause of such failure instances.

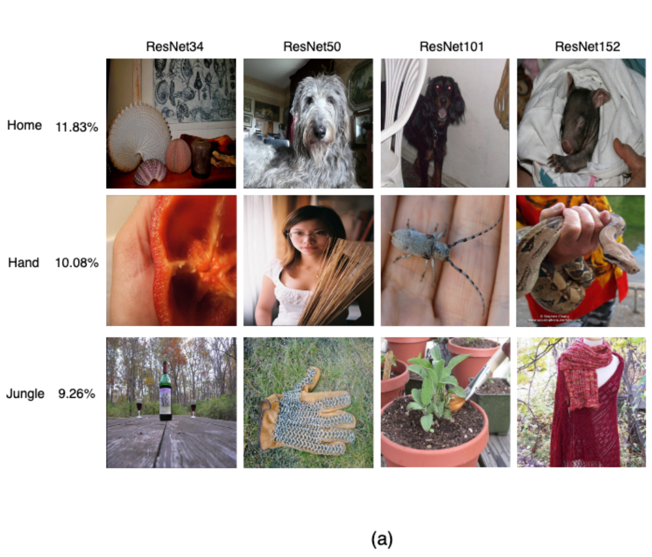

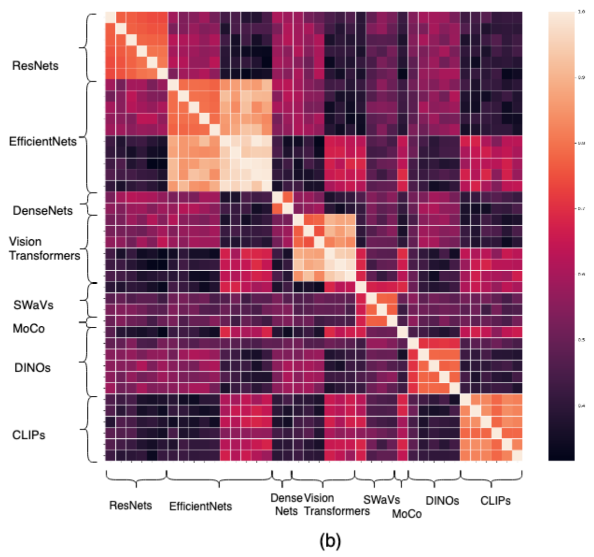

Figure 4: a) The most three common failure backgrounds in ResNets pretrained on ImageNet. The numbers in the image show the percentage of the shared failures that are related to the mentioned background. b) Comparing failures of all models **(Intersection/Union)**.We observe that models belonging to the same categories tend to exhibit more comparable failures.

5.2.2 Collective Failure Inspection

Within this section, we will compare the failure modes for all models to assess their alignment. We aim to determine the extent to which failures are consistent across models. While numerous studies have focused on analyzing similarities in the learning process and representations of different models, such as Raghu et al. (2021) that demonstrated the similarity between convolutional neural networks (convnets) and other convnets, as well as the similarity between vision transformers (ViTs) and other ViTs int the way they learn features, our focus is on investigating whether models also fail in similar ways. This will enable us to gain a deeper understanding of how to address the issue of failures in a more generalized manner without taking the specific model into consideration.

The failures of different models in various categories are compared in Figure 4 by computing the *intersection over union* of the failures. It can be observed that models within the same category fail in more similar samples. Typically, the failures between models from the same category are over 80% similar (e.g., CLIPs and EfficientNets). Among all 40 models, the intersection of failure modes is above 40%, indicating that models tend to fail in very similar ways, even with different architectures. Some examples of the shared failures relted to backgrounds can be found in 4. This will raise the question of "how to utilize this similarity in failures to enhance a group of models' performance?" which we will explore more in section 5.3.2.

It is pertinent to mention that Wiles et al. (2022) has also recognized patterns of consistencies in failures among models within the same category. However, we take a step further and leverage these consistencies to mitigate shared failure modes systematically.

5.3 Failure Mitigation

5.3.1 Individual Failure Mitigation

The outcomes from employing our framework are presented in Table 2. We only included the results for ResNets and DINOs, but we have results for other models (EfficientNets, DenseNets, ViTs, SWaVs, MoCo, and CLIPs) in the appendix. In Table 2, we constructed ***DebugSeed*** and ***DebugHeldout*** sets to yield zero accuracy for the model, as they are composed of model failures. Post refinement and utilizing ***DebugSeed***, we observe substantial improvements in ***DebugHeldout*** data that we did not use for refinement, ensuring an

Models	Accuracies					
Model category	model name	**Individual Refinement (ours)**				Random Refinement	
		Clean	Failure	Seed	**Heldout**	Seed	Heldout
ResNet	ResNet18	0.9891	0.0651	0.2636	**0.2128**	0.1134	0.1129
	ResNet26	0.9783	0.0649	0.2856	**0.228**	0.09539	0.0904
	ResNet34	0.9879	0.0781	0.3061	**0.2531**	0.09856	0.08615
	ResNet50	0.9864	0.0607	0.3444	**0.2717**	0.1102	0.1072
	ResNet101	0.9790	0.113	0.3574	**0.2656**	0.1132	0.1181
	ResNet152	0.9901	0.0863	0.3609	**0.2817**	0.08207	0.08804
DINO	ViT-S/8	0.9812	0.0536	0.3117	**0.2494**	0.1134	0.1129
	ViT-S/16	0.9855	0.0462	0.2922	**0.2379**	0.09539	0.0904
	ViT-B/8	0.9782	0.0655	0.3325	**0.2518**	0.09856	0.08615
	ViT-B/16	0.9848	0.0388	0.3067	**0.2477**	0.1102	0.1072

Table 2: Our approach significantly outperforms Random Refinement, leading to an approximate $\sim 21\%$ improvement in accuracy across all models on the ***DebugHeldout*** dataset. This underscores the effectiveness of our method in rectifying errors attributed to incorrect background associations. Clean and Failure accuracies reflect the post-refinement performance of correctly and incorrectly classified data, respectively, which show that our method do not harm the clean accuracy by incorporating additional data. Prior to refinement, models exhibited zero accuracy on ***DebugSeed*** and ***DebugHeldout*** datasets.

unbiased evaluation. This improvement underscores that many failure modes stem from incorrect associations models make between objects and backgrounds. Some might argue that this gain results from the additional data. Thus, we present results for a baseline we term **Random refinement**. This baseline similarly uses ***DebugSeed*** and ***DebugHeldout***, then generates synthetic data using only class names (prompts are structured as *"A photo of [class_name]"*). This comparison illustrates that the improvement of our method arises from considering background information. In the outcomes of **Random refinement**, the improvement over ***DebugSeed*** and ***DebugHeldout*** is roughly equivalent since no information from the background association of either set was utilized. **Random refinement** solely employs class names to generate data. However, this improvement is not on par with the gain achieved by incorporating background information when generating new data. We also include results for Color spurious associations on CIFAR-100 in table 3 to further support our claim. Results for iNaturalist-2018 can also be found in table 8.

It's worth noting that despite incorporating Stable Diffusion-generated data, which could be seen as out-of-distribution samples, a positive impact on model performance remains. This is primarily attributed to the parameter ***lambda*** that controls the contribution of the generated images in our training process. The influence of this parameter is depicted in Figure 5.

Another crucial hyper-parameter is the number (#) of generated synthetic data per class. The effect of this hyper-parameter, denoted as ***k***, is illustrated in Figure 5.

The improvement observed in ***DebugHeldout*** surpasses $\sim 21\%$ for all models, highlighting the tendency of models to fail in associating backgrounds with objects and utilizing this association to predict objects, neglecting object-specific features. This can be contrasted with the accuracy gain achieved by the **Random refinement** baseline, which is significantly smaller than our method. We also include results of comparing our framework with other methods such as Jain et al. (2023); Yun et al. (2019); Singla et al. (2024) in section B in appendix. The results show the superiority of our spurious correlation identification and mitigation framework comparing to other related work.

5.3.2 Collective Failure Mitigation

As discussed in section 5.2.2, since models from the same categories have very similar failures, we have considered the possibility of using a single set of generated data, called ***Collective_DebugTrain***, to refine

Models	Accuracies						
Model category	model name	**Individual Refinement** (ours)				Random Refinement	
		Clean	Failure	Seed	Heldout	Seed	Heldout
ResNet	ResNet18	0.9892	0.1305	0.3323	**0.2818**	0.1901	0.1878
	ResNet34	0.9952	0.1560	0.3586	**0.2923**	0.1902	0.1947
	ResNet50	0.9931	0.1394	0.3614	**0.3008**	0.1971	0.1858
	ResNet101	0.9991	0.169	0.3877	**0.3249**	0.2001	0.1930
	ResNet152	0.9943	0.1525	0.3842	**0.3184**	0.2139	0.2152

Table 3: Accuracy of our method compared to the Random refinement on CIFAR-100 considering color spurious correlations. The prompt used in the above table to input ChatGPT is "What is an uncommon color that <class_name> may possess?", and the prompt for generating more data with Stable Diffusion is "A photo of a <color> <class_name>.". Note that the accuracy of models on ***DebugSeed*** and ***DebugHeldout*** was zero before refinement. After applying our method, we gain above $\sim 28\%$ improvements in accuracies for all models, showcasing that more than $\sim 28\%$ of model errors in the heldout set come from wrong color associations.

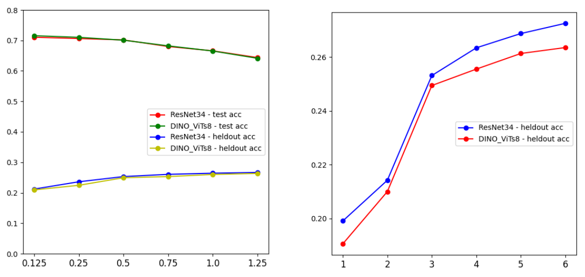

(a) Effect of hyper parameter lambda on both test and heldout accuracies.

(b) Effect of hyper-parameter k (# chosen backgrounds per class) on heldout accuracy

Figure 5: a) As the value of ***lambda*** increases, the accuracy on ***DebugHeldout*** improves while the accuracy on the test set (containing both clean and failure examples) decreases, meaning increasing lambda by a certain value will harm the clean accuracy. However, there is a specific point **(0.5)** on the plot where the accuracy of the models on both the test and heldout sets stabilizes. b) Increasing the number of chosen backgrounds per class enhances the accuracy on the ***DebugHeldout***. Considering the high cost of generating additional data, we opt for $\mathbf{k = 3}$, where the plot exhibits a significant slope, and the few-shot generation of additional data will help in accuracy improvement.

all models within the same categories. To achieve this, we have devised two different settings: 1) we get the failure modes of all models in the same category (e.g. ResNets), and we select ***k*** samples from all the failures in each class. Therefore, background failures that occurred more have a higher probability of being chosen for the ***Collective_DebugTrain***. We then use this data to refine individual models in this category. 2) We get the failure modes of only one of the models in a category and then use this to refine all models. This approach is more efficient in terms of time and memory, as it requires running only one model per category. The results for this experiment are shown in table 4. Based on our observations in section 5.2.2, having the same ***DebugTrain*** data for refinement (***Collective_DebugTrain***), improves the accuracies among all models in the same category. This approach offers greater efficiency as it eliminates the need to generate ***DebugTrain*** data for each individual model. Consequently, it saves us both time and memory that would otherwise be required for storing such data.

In an overview, the **collective refinement** approach showcases the capability to resolve above **75%** of failures corrected by individual refinement 6.

Models		Accuracies							
Model category	model name	Before debugging	**Collective refinement-type 1** (ours)			**Collective refinement-type 2** (ours)			
		Test	Test	seed	**heldout**	Test	seed	**heldout**	
ResNet	ResNet18	0.6236	0.6364	0.2291	**0.2078**	0.6413	0.2636	**0.2128**	
	ResNet26	0.6593	0.6655	0.2396	**0.2192**	0.6669	0.2185	**0.1853**	
	ResNet34	0.7017	0.7149	0.2312	**0.2188**	0.7135	0.2391	**0.2178**	
	ResNet50	0.7631	0.7644	0.2419	**0.2217**	0.7641	0.2325	**0.2105**	
	ResNet101	0.796	0.8001	0.2474	**0.2226**	0.7999	0.2244	**0.2045**	
	ResNet152	0.816	0.8182	0.2509	**0.2317**	0.8188	0.2253	**0.2081**	
DINO	ViT-S/8	0.6977	0.70001	0.2729	**0.2488**	0.70008	0.3117	**0.2494**	
	ViT-S/16	0.649	0.6522	0.2673	**0.2394**	0.6504	0.2563	**0.2267**	
	ViT-B/8	0.7101	0.7125	0.2913	**0.2509**	0.7117	0.2903	**0.2540**	
	ViT-B/16	0.6832	0.6840	0.2985	**0.2467**	0.6833	0.2855	**0.2488**	

Table 4: Collective refinement results.

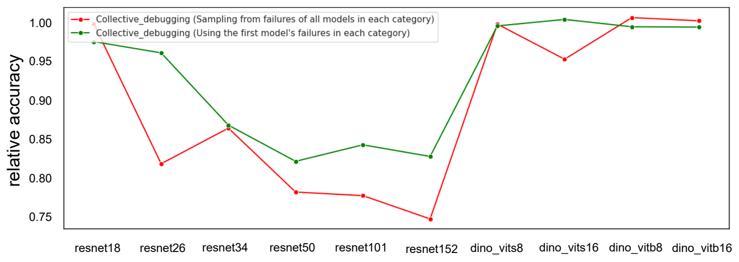

Figure 6: Comparison of resolved failures between collective refinement and individual refinement as a percentage. Relative accuracy is the ratio of the collective refinement's accuracy over individual refinement's accuracy on each specific model. Our **collective refinement** method is able to resolve more than 75% of individual model's failures.

6 Conclusion

In this project, we have developed a technique to identify failure modes by focusing on a specific category of spurious correlations. We then leverage these detected failures to generate additional samples, allowing the model to learn from and address its shortcomings. We have illustrated the resemblance of failures within a particular model category, highlighting that models with the same architecture share more similar failures. Exploiting this insight, we have devised a method to alleviate failures across all models in a category using a single set of generated data based on the failures of just one model in that category. Our results indicate that **collective refinement** approach can resolve over 75% of failures addressed through **individual refinement** efforts. Our framework empowers users to select the spurious correlation to identify and mitigate, facilitating the simultaneous refinement of a subset of models with a single (small) auxiliary set of additional data, thereby saving both time and resource.

7 Discussion

Failure modes of Stable Diffusion: Prior work have investigated failure modes of diffusion-based models. Liu et al. (2023) proposes SAGE, an adversarial search method that explores failure modes in Text-Guided Diffusion Models (TDMs), revealing issues like generating inaccurate images and identifying misalignments between latent and prompt spaces. Some other work explore the problem of compositionality in Text-Guided generative models by using manually crafted prompts, including Gokhale et al. (2022); Marcus et al. (2022); Conwell & Ullman (2023). Another line of work have studied biases in generative models including societal biases Luccioni et al. (2023); Saravanan et al. (2023) and gender biases Wu et al. (2023). While these studies highlight significant challenges and shortcomings in text-to-image generative models, it is important to note that, for the practical purpose of automatic generation, these models remain a widely adopted approach, and are currently represent the most effective solution available for automated content generation.

References

Devansh Arpit, Stanisław Jastrzębski, Nicolas Ballas, David Krueger, Emmanuel Bengio, Maxinder S Kanwal, Tegan Maharaj, Asja Fischer, Aaron Courville, Yoshua Bengio, et al. A closer look at memorization in deep networks. In *International conference on machine learning*, pp. 233–242. PMLR, 2017.

Hritik Bansal and Aditya Grover. Leaving reality to imagination: Robust classification via generated datasets. *arXiv preprint arXiv:2302.02503*, 2023.

Andrei Barbu, David Mayo, Julian Alverio, William Luo, Christopher Wang, Dan Gutfreund, Josh Tenenbaum, and Boris Katz. Objectnet: A large-scale bias-controlled dataset for pushing the limits of object recognition models. *Advances in neural information processing systems*, 32, 2019.

Tim Brooks, Aleksander Holynski, and Alexei A Efros. Instructpix2pix: Learning to follow image editing instructions. In *Proceedings of the IEEE/CVF Conference on Computer Vision and Pattern Recognition*, pp. 18392–18402, 2023.

Mathilde Caron, Ishan Misra, Julien Mairal, Priya Goyal, and Piotr Bojanowski. Unsupervised learning of visual features by contrasting cluster assignments. In *European Conference on Computer Vision*, pp. 116–132. Springer, 2020.

Mathilde Caron, Hugo Touvron, Ishan Misra, Hervé Jégou, Julien Mairal, Piotr Bojanowski, and Armand Joulin. Emerging properties in self-supervised vision transformers. In *Proceedings of the IEEE/CVF international conference on computer vision*, pp. 9650–9660, 2021.

Xiaozhi Chen, Kaustav Kundu, Zhiqiang Zhang, Huimin Ma, Sanja Fidler, and Raquel Urtasun. 3d object proposals for accurate object class detection. In *Advances in Neural Information Processing Systems*, pp. 2146–2156, 2018.

Yeounoh Chung, Tim Kraska, Neoklis Polyzotis, Ki Hyun Tae, and Steven Euijong Whang. Slice finder: Automated data slicing for model validation. In *2019 IEEE 35th International Conference on Data Engineering (ICDE)*, pp. 1550–1553. IEEE, 2019.

Colin Conwell and Tomer Ullman. A comprehensive benchmark of human-like relational reasoning for text-to-image foundation models. In *ICLR 2023 Workshop on Mathematical and Empirical Understanding of Foundation Models*, 2023.

Alexey Dosovitskiy, Lucas Beyer, Alexander Kolesnikov, Dirk Weissenborn, Xiaohua Zhai, Thomas Unterthiner, Mostafa Dehghani, Matthias Minderer, Georg Heigold, Sylvain Gelly, et al. An image is worth 16x16 words: Transformers for image recognition at scale. In *Proceedings of the IEEE/CVF Conference on Computer Vision and Pattern Recognition*, pp. 10687–10698, 2021.

Sabri Eyuboglu, Maya Varma, Khaled Saab, Jean-Benoit Delbrouck, Christopher Lee-Messer, Jared Dunnmon, James Zou, and Christopher Ré. Domino: Discovering systematic errors with cross-modal embeddings. *International Conference on Learning Representations (ICLR)*, 2022.

Tejas Gokhale, Hamid Palangi, Besmira Nushi, Vibhav Vineet, Eric Horvitz, Ece Kamar, Chitta Baral, and Yezhou Yang. Benchmarking spatial relationships in text-to-image generation. *arXiv preprint arXiv:2212.10015*, 2022.

Kaiming He, Xiangyu Zhang, Shaoqing Ren, and Jian Sun. Deep residual learning for image recognition. In *Proceedings of the IEEE Conference on Computer Vision and Pattern Recognition*, pp. 770–778, 2016.

Kaiming He, Haoqi Fan, Yuxin Wu, Saining Xie, and Ross Girshick. Momentum contrast for unsupervised visual representation learning. In *Proceedings of the IEEE Conference on Computer Vision and Pattern Recognition*, pp. 9729–9738, 2019.

Dan Hendrycks and Thomas Dietterich. Benchmarking neural network robustness to common corruptions and perturbations. *International Conference on Learning Representations (ICLR)*, 2019.

Dan Hendrycks, Steven Basart, Norman Mu, Saurav Kadavath, Frank Wang, Evan Dorundo, Rahul Desai, Tyler Zhu, Samyak Parajuli, Mike Guo, et al. The many faces of robustness: A critical analysis of out-of-distribution generalization. In *Proceedings of the IEEE/CVF International Conference on Computer Vision*, pp. 8340–8349, 2021a.

Dan Hendrycks, Kevin Zhao, Steven Basart, Jacob Steinhardt, and Dawn Song. Natural adversarial examples. In *Proceedings of the IEEE/CVF Conference on Computer Vision and Pattern Recognition*, pp. 15262–15271, 2021b.

Chunsan Hong, Byunghee Cha, Bohyung Kim, and Tae-Hyun Oh. Enhancing classification accuracy on limited data via unconditional gan. In *Proceedings of the IEEE/CVF International Conference on Computer Vision*, pp. 1057–1065, 2023.

Gao Huang, Zhuang Liu, Laurens Van Der Maaten, and Kilian Q Weinberger. Densely connected convolutional networks. In *Proceedings of the IEEE Conference on Computer Vision and Pattern Recognition*, pp. 4700–4708, 2017.

Saachi Jain, Hannah Lawrence, Ankur Moitra, and Aleksander Madry. Distilling model failures as directions in latent space. *International Conference on Learning Representation (ICLR)*, 2023.

Lu Jiang, Dong Meng, Ioannis Mitliagkas, and J. Zico Kolter. Mentornet: Learning data-driven curriculum for very deep neural networks on corrupted labels. In *Advances in Neural Information Processing Systems*, pp. 10154–10163, 2018.

Priyatham Kattakinda and Soheil Feizi. Focus: Familiar objects in common and uncommon settings. *arXiv preprint arXiv:2110.03804*, 2021.

Priyatham Kattakinda, Alexander Levine, and Soheil Feizi. Invariant learning via diffusion dreamed distribution shifts. *arXiv preprint arXiv:2211.10370*, 2022.

Bahjat Kawar, Shiran Zada, Oran Lang, Omer Tov, Huiwen Chang, Tali Dekel, Inbar Mosseri, and Michal Irani. Imagic: Text-based real image editing with diffusion models. In *Proceedings of the IEEE/CVF Conference on Computer Vision and Pattern Recognition*, pp. 6007–6017, 2023.

Soroush Abbasi Koohpayegani, Anuj Singh, KL Navaneet, Hadi Jamali-Rad, and Hamed Pirsiavash. Genie: Generative hard negative images through diffusion. *arXiv preprint arXiv:2312.02548*, 2023.

Qihao Liu, Adam Kortylewski, Yutong Bai, Song Bai, and Alan Yuille. Intriguing properties of text-guided diffusion models. *arXiv preprint arXiv:2306.00974*, 2023.

Jiasen Lu, Dhruv Batra, Devi Parikh, and Stefan Lee. Vilbert: Pretraining task-agnostic visiolinguistic representations for vision-and-language tasks. In *Advances in Neural Information Processing Systems*, pp. 13–23, 2019.

Alexandra Sasha Luccioni, Christopher Akiki, Margaret Mitchell, and Yacine Jernite. Stable bias: Analyzing societal representations in diffusion models. *arXiv preprint arXiv:2303.11408*, 2023.

Lorenzo Luzi, Ali Siahkoohi, Paul M Mayer, Josue Casco-Rodriguez, and Richard Baraniuk. Boomerang: Local sampling on image manifolds using diffusion models. *arXiv preprint arXiv:2210.12100*, 2022.

Gary Marcus, Ernest Davis, and Scott Aaronson. A very preliminary analysis of dall-e 2. *arXiv preprint arXiv:2204.13807*, 2022.

Chenlin Meng, Yutong He, Yang Song, Jiaming Song, Jiajun Wu, Jun-Yan Zhu, and Stefano Ermon. Sdedit: Guided image synthesis and editing with stochastic differential equations. *arXiv preprint arXiv:2108.01073*, 2021.

Eric Mitchell, Charles Lin, Antoine Bosselut, Chelsea Finn, and Christopher D Manning. Fast model editing at scale. *arXiv preprint arXiv:2110.11309*, 2021.

Nilaksh Mithun, Soubhik Biswas, and CV Jawahar. Neural modular network for visual reasoning. In *Proceedings of the IEEE/CVF Conference on Computer Vision and Pattern Recognition*, pp. 13306–13315, 2020.

Ron Mokady, Amir Hertz, Kfir Aberman, Yael Pritch, and Daniel Cohen-Or. Null-text inversion for editing real images using guided diffusion models. In *Proceedings of the IEEE/CVF Conference on Computer Vision and Pattern Recognition*, pp. 6038–6047, 2023.

Besmira Nushi, Ece Kamar, and Eric Horvitz. Towards accountable ai: Hybrid human-machine analyses for characterizing system failure. In *Proceedings of the AAAI Conference on Human Computation and Crowdsourcing*, volume 6, pp. 126–135, 2018.

Alec Radford, Jong Wook Kim, Chris Hallacy, Aditya Ramesh, Gabriel Goh, Sandhini Agarwal, Girish Sastry, Amanda Askell, Pamela Mishkin, Jack Clark, et al. Learning transferable visual models from natural language supervision. In *International conference on machine learning*, pp. 8748–8763. PMLR, 2021.

Maithra Raghu, Thomas Unterthiner, Simon Kornblith, Chiyuan Zhang, and Alexey Dosovitskiy. Do vision transformers see like convolutional neural networks? *Advances in Neural Information Processing Systems*, 34:12116–12128, 2021.

Alexandre Rame, Matthieu Kirchmeyer, Thibaud Rahier, Alain Rakotomamonjy, Patrick Gallinari, and Matthieu Cord. Diverse weight averaging for out-of-distribution generalization. *arXiv preprint arXiv:2205.09739*, 2022.

Scott Reed, Honglak Lee, Dragomir Anguelov, Christian Szegedy, Dumitru Erhan, and Andrew Rabinovich. Training deep neural networks on noisy labels with bootstrapping. In *International Conference on Learning Representations (ICLR)*, 2015.

Marco Tulio Ribeiro, Sameer Singh, and Carlos Guestrin. " why should i trust you?" explaining the predictions of any classifier. In *Proceedings of the 22nd ACM SIGKDD international conference on knowledge discovery and data mining*, pp. 1135–1144, 2016.

Robin Rombach, Andreas Blattmann, Dominik Lorenz, Patrick Esser, and Björn Ommer. High-resolution image synthesis with latent diffusion models. 2022 ieee. In *CVF Conference on Computer Vision and Pattern Recognition (CVPR)*, pp. 10674–10685, 2021.

Shiori Sagawa, Pang Wei Koh, Tatsunori B Hashimoto, and Percy Liang. Distributionally robust neural networks for group shifts: On the importance of regularization for worst-case generalization. *International Conference on Learning Representations (ICLR)*, 2020.

Shibani Santurkar, Dimitris Tsipras, Mahalaxmi Elango, David Bau, Antonio Torralba, and Aleksander Madry. Editing a classifier by rewriting its prediction rules. *Advances in Neural Information Processing Systems*, 34:23359–23373, 2021.

Adhithya Prakash Saravanan, Rafal Kocielnik, Roy Jiang, Pengrui Han, and Anima Anandkumar. Exploring social bias in downstream applications of text-to-image foundation models. *arXiv preprint arXiv:2312.10065*, 2023.

Sahil Singla and Soheil Feizi. Salient imagenet: How to discover spurious features in deep learning? *International Conference on Learning Representations (ICLR)*, 2022.

Sahil Singla, Besmira Nushi, Shital Shah, Ece Kamar, and Eric Horvitz. Understanding failures of deep networks via robust feature extraction. In *Proceedings of the IEEE/CVF Conference on Computer Vision and Pattern Recognition*, pp. 12853–12862, 2021.

Sahil Singla, Atoosa Malemir Chegini, Mazda Moayeri, and Soheil Feizi. Data-centric debugging: mitigating model failures via targeted image retrieval. In *Proceedings of the IEEE/CVF Winter Conference on Applications of Computer Vision*, pp. 63–74, 2024.

Sainbayar Sukhbaatar, Joan Bruna, Manohar Paluri, and Rob Fergus. Training convolutional networks with noisy labels. In *Advances in Neural Information Processing Systems (NIPS)*, pp. 468–476, 2014.

Mingxing Tan and Quoc V Le. Efficientnet: Rethinking model scaling for convolutional neural networks. *arXiv preprint arXiv:1905.11946*, 2019.

Patrick von Platen, Suraj Patil, Anton Lozhkov, Pedro Cuenca, Nathan Lambert, Kashif Rasul, Mishig Davaadorj, and Thomas Wolf. Diffusers: State-of-the-art diffusion models. URL `https://github.com/huggingface/diffusers`.

Olivia Wiles, Isabela Albuquerque, and Sven Gowal. Discovering bugs in vision models using off-the-shelf image generation and captioning. *arXiv preprint arXiv:2208.08831*, 2022.

Eric Wong, Shibani Santurkar, and Aleksander Madry. Leveraging sparse linear layers for debuggable deep networks. In *International Conference on Machine Learning*, pp. 11205–11216. PMLR, 2021.

Tongshuang Wu, Marco Tulio Ribeiro, Jeffrey Heer, and Daniel S Weld. Errudite: Scalable, reproducible, and testable error analysis. In *Proceedings of the 57th Annual Meeting of the Association for Computational Linguistics*, pp. 747–763, 2019.

Yankun Wu, Yuta Nakashima, and Noa Garcia. Stable diffusion exposed: Gender bias from prompt to image. *arXiv preprint arXiv:2312.03027*, 2023.

Kai Xiao, Logan Engstrom, Andrew Ilyas, and Aleksander Madry. Noise or signal: The role of image backgrounds in object recognition. *International Conference on Learning Representations (ICLR)*, 2021.

Moon Ye-Bin, Nam Hyeon-Woo, Wonseok Choi, Nayeong Kim, Suha Kwak, and Tae-Hyun Oh. Exploiting synthetic data for data imbalance problems: Baselines from a data perspective. *arXiv preprint arXiv:2308.00994*, 2023.

Sangdoo Yun, Dongyoon Han, Seong Joon Oh, Sanghyuk Chun, Junsuk Choe, and Youngjoon Yoo. Cutmix: Regularization strategy to train strong classifiers with localizable features. In *Proceedings of the IEEE/CVF international conference on computer vision*, pp. 6023–6032, 2019.

Jianguo Zhang, Marcin Marszałek, Svetlana Lazebnik, and Cordelia Schmid. Local features and kernels for classification of texture and object categories: A comprehensive study. *International journal of computer vision*, 73:213–238, 2007.

Jiawei Zhang, Yang Wang, Piero Molino, Lezhi Li, and David S Ebert. Manifold: A model-agnostic framework for interpretation and diagnosis of machine learning models. *IEEE transactions on visualization and computer graphics*, 25(1):364–373, 2018a.

Min-Ling Zhang, Xingquan Wu, and Zhi-Hua Zhou. Multi-label learning with missing labels: A probabilistic perspective. *IEEE Transactions on Knowledge and Data Engineering*, 30(3):504–517, 2018b.

Zhixing Zhang, Ligong Han, Arnab Ghosh, Dimitris N Metaxas, and Jian Ren. Sine: Single image editing with text-to-image diffusion models. In *Proceedings of the IEEE/CVF Conference on Computer Vision and Pattern Recognition*, pp. 6027–6037, 2023.

Chenyu Zheng, Guoqiang Wu, and Chongxuan Li. Toward understanding generative data augmentation. *arXiv preprint arXiv:2305.17476*, 2023.

Bowen Zhou, Yanhua Wu, Bingbing Ni, Xueying Zhou, Jing Wen, and Jie Zou. Towards mitigating bias in deep learning-based automated skin lesion classification with balanced groups and label correction. *IEEE Journal of Biomedical and Health Informatics*, 24(10):2803–2813, 2020.

Yongchao Zhou, Hshmat Sahak, and Jimmy Ba. Training on thin air: Improve image classification with generated data. *arXiv preprint arXiv:2305.15316*, 2023.

A Appendix

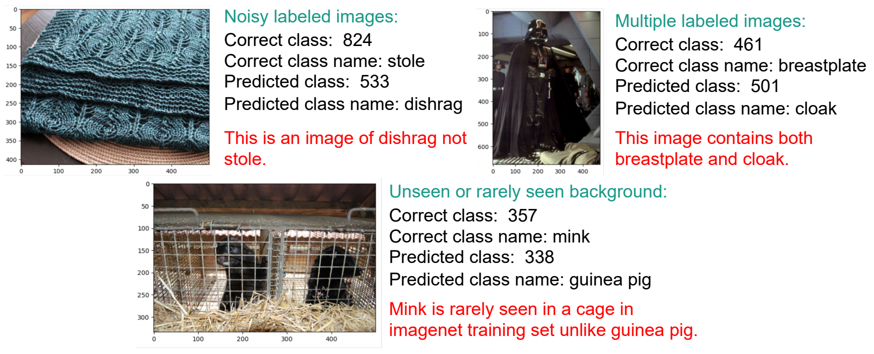
Noisy labeled images:
Correct class: 824
Correct class name: stole
Predicted class: 533
Predicted class name: dishrag
This is an image of dishrag not stole.

Multiple labeled images:
Correct class: 461
Correct class name: breastplate
Predicted class: 501
Predicted class name: cloak
This image contains both breastplate and cloak.

Unseen or rarely seen background:
Correct class: 357
Correct class name: mink
Predicted class: 338
Predicted class name: guinea pig
Mink is rarely seen in a cage in imagenet training set unlike guinea pig.

Figure 7: examples of 3 most common failure modes of deep learning models

Parameter	Value
Leearning rate	0.2
Epochs	1000
Momentum	0.9
Weight decay	0.0005
# Chosen common BGs	3
lambda	0.5

Table 5: Shared parameters among all dataset.

Models			
Model_category	Model_name		
ResNet	ResNet18 ResNet50	ResNet26 ResNet101	ResNet34 ResNet152
EfficientNet	efficientnet_b0 efficientnet_b3 efficientnet_b6 efficientnet_l2	efficientnet_b1 efficientnet_b4 efficientnet_b7	efficientnet_b2 efficientnet_b5 efficientnet_b8
DenseNet	densenet121	densenet161	
ViT	vit_base_patch16_224 vit_large_patch32_224	vit_base_patch32_224 vit_base_resnet26d_224	vit_large_patch16_224 vit_base_resnet50d_224
SWaV	resnet50 resnet50w5	resnet50w2	resnet50w4
MoCo	moco_v2_800ep		
DINO	dino_resnet50 dino_vits16	dino_vitb16 dino_vits8	dino_vitb8
CLIP	ViT-B32 ViT-L14	RN50	RN101

Table 6: List of models we tested our refinement framework on.

Models	Accuracies							
Model category	model name	before refinement	**Individual refinement** (ours)			Random refinement		
		Test	Test	seed	**heldout**	Test	seed	heldout
EfficientNet	b0	0.715	0.7198	0.2034	**0.1842**	0.7134	0.0894	0.0883
	b1	0.7373	0.74415	0.2154	**0.1885**	0.7399	0.1003	0.1011
	b2	0.7525	0.7591	0.2283	**0.1909**	0.7448	0.0957	0.0942
	b3	0.7634	0.7730	0.2318	**0.1991**	0.7669	0.1066	0.1010
	b4	0.7701	0.7780	0.2398	**0.2068**	0.7719	0.0955	0.0960
	b5	0.7821	0.7819	0.2405	**0.2055**	0.7761	0.0893	0.0915
	b6	0.7884	0.7886	0.2561	**0.2083**	0.7863	0.0941	0.0914
	b7	0.7895	0.7903	0.2600	**0.2126**	0.7898	0.0951	0.0972
	b8	0.7928	0.7951	0.2653	**0.2147**	0.7932	0.0972	0.0934
DenseNet	121	0.6792	0.6869	0.2138	**0.1592**	0.6773	0.0651	0.0664
	161	0.7254	0.7332	0.2418	**0.1833**	0.7249	0.0779	0.0771
ViT	base_patch16_224	0.739	0.7477	0.2501	**0.2193**	0.7399	0.1047	0.1044
	base_patch32_224	0.7456	0.7493	0.2574	**0.2199**	0.7469	0.1078	0.1072
	large_patch16_224	0.7493	0.7539	0.2644	**0.2263**	0.7468	0.0952	0.0957
	large_patch32_224	0.7535	0.7545	0.2674	**0.2274**	0.7553	0.1023	0.1041
SWaV	resnet50	0.4254	0.4384	0.1403	**0.1274**	0.4267	0.0662	0.0624
	resnet50w2	0.4317	0.4328	0.1583	**0.1294**	0.4319	0.0683	0.0652
	resnet50w4	0.4402	0.4477	0.1592	**0.1304**	0.4416	0.0672	0.0617
	resnet50w5	0.4526	0.4589	0.1633	**0.1363**	0.4552	0.0696	0.0703
MoCo	v2_800ep	0.6931	0.6946	0.2041	**0.1584**	0.6937	0.0943	0.0917
CLIP	ViT-B32	0.5388	0.5582	0.1794	**0.1635**	0.5407	0.0776	0.0763
	ViT-L14	0.7427	0.7694	0.2174	**0.2068**	0.7505	0.0893	0.0981
	RN50	0.5928	0.6129	0.1980	**0.1833**	0.6004	0.0964	0.0946
	RN101	0.7532	0.7751	0.2566	**0.2142**	0.7570	0.1084	0.1115

Table 7: Accuracy of our method comparing to **Random refinement**. Note that the accuracy of models on ***DebugSeed*** and ***DebugHeldout*** was zero before refinement.

Models	Accuracies							
Model category	model name	Accuracy before debugging	**Accuracy of Individual Debugging** (ours)			Accuracy of Random debugging		
		Test	Test	seed	**heldout**	Test	seed	heldout
ResNet	ResNet50	0.7581	0.7852	0.3612	**0.3082**	0.7614	0.1348	0.1352
	ResNet101	0.7863	0.8148	0.3910	**0.3173**	0.7899	0.1377	0.1384
	ResNet152	0.7996	0.8252	0.3916	**0.3194**	0.8015	0.1485	0.1463

Table 8: Accuracy of our method compared to the **Random refinement** on iNaturalist-2018 considering background spurious correlations. Note that the accuracy of models on ***DebugSeed*** and ***DebugHeldout*** was zero before refinement.

To better compare the superiority of using ChatGPT for uncommon spurious correlation suggestion, we include the accuracy improvement on ImageNet for mitigating background associations when using a pre-defined set of backhgrounds which contain ["in a blur background", "on a leaf", "in water", "on soil", "on a plate", "in a hand", "on a sofa", "in garden", "in jungle", "in cave", "on snow", "in a plane background", "in yard", "outdoor", "in shore", "in the sky", "indoor", "on a wall", "on a tree", "on a table", "in a street", "on a rock", "in a airplane", "in cage", "with sun", "in a mountain", "in metro", "on grass", "in shelf", "on rails",

Models		Accuracies	
Model category	model name	**Accuracy of Individual Debugging** (ours)	
		seed	**heldout**
ResNet	ResNet18	0.2260	**0.1690**
	ResNet26	0.2295	**0.1751**
	ResNet34	0.2294	**0.1788**
	ResNet50	0.2354	**0.1806**
	ResNet101	0.2384	**0.1847**
	ResNet152	0.2402	**0.1857**
DINO	ViT-S/8	0.2310	**0.2073**
	ViT-S/16	0.2231	**0.2044**
	ViT-B/8	0.2492	**0.2271**
	ViT-B/16	0.2359	**0.2118**

Table 9: Accuracy of our method when using a set of pre-defined backgrounds to mitigate background spurious correlations in ImageNet dataset. Results show the superiority of using ChatGPT for rare background suggestion.

"with a person", "on bed", "in a playground", "in a kitchen", "on floor", "on glass", "on wood", "at a party", "in a wardrobe", "in a restaurant", "in a bucket"]. The results for this experiment can be seen in table 9.

B Comparing to baselines

B.1 CutMix Yun et al. (2019)

Method: The CutMix augmentation strategy is proposed to improve regional dropout methods for training convolutional neural network classifiers. Instead of removing informative pixels with patches of black pixels or random noise, CutMix involves cutting and pasting patches among training images, with ground truth labels mixed proportionally to the patch area. This approach efficiently utilizes training pixels while retaining the regularization effect of regional dropout.

Setting: We employ the implementation provided by the authors of the paper. The pretrained models were trained using the below configuration:

Parameter	**Value**
`net_type`	`resnet`
`dataset`	`imagenet`
`batch_size`	`256`
`lr`	`0.1`
`depth`	`50`
`epochs`	`300`
`expname`	`ResNet50`
`j`	`40`
`beta`	`1.0`
`cutmix_prob`	`1.0`
`verbose`	No

Table 10: CutMix experiment configuration on ImageNet (e.g., ResNet50)

B.2 Jain et al. (2023)

Method: They automatically distill failure modes in machine learning models to offer a global understanding of datasets. The method involves representing failure modes as directions in a feature space by training linear classifiers. This allows for the automatic detection, interpretation, and intervention of model failures. Shared vision/language embeddings like CLIP are leveraged to ensure consistency.

Setting: We use the official GitHub implementation provided by the paper. All the settings, including the percentage of validation set and ***DebugSet***, are the same as ours. We compare their result with ours on ***DebugHeldout*** in table 11.

B.3 DCD Singla et al. (2024)

Method: DCD addresses model failures in deep neural networks, particularly in scenarios where the training set inadequately covers diverse deployment settings. Focusing on image classification, DCD leverages a small set of samples from an error distribution (Esample) and a large pool of weakly labeled data (F). The framework systematically improves model performance on the error distribution while maintaining accuracy on the original test set. DCD strategically selects visually similar images from F by using the $l2$ distance in the penultimate layer activations of various models.

Comparison: Since the paper's code is not available, the frameworks are compared based on their methods to find and mitigate failures.

- The identified failures lack interpretability, a crucial aspect for sanity checks and gaining deeper insights into the models' behaviors.
- The method involves a time-consuming manual process, including the selection of a subset of classes with low accuracy, gathering synsets, and performing a Flickr search for synonyms. This results in collecting a substantial number of image URLs (e.g., 952,951 across 160 ImageNet classes) and adds complexity by removing common URLs across classes. In contrast, our method only adds **3** images per class, significantly reducing the additional data burden.

In table 11, we compare our results with Jain et al. (2023); Yun et al. (2019). Note that the final models are all tested on the same ***DebugHeldout*** for a fair comparison.

Models	Accuracies on ***DebugHeldout***			
Model Category	model name	**Ours**	Jain et al. (2023)	Yun et al. (2019) CutMix
ResNet	ResNet18	**0.2128**	0.0923	0.0642
	ResNet26	**0.228**	0.1023	0.0527
	ResNet34	**0.2531**	0.0839	0.0655
	ResNet50	**0.2717**	0.1185	0.0738
	ResNet101	**0.2656**	0.1147	0.0870
	ResNet152	**0.2817**	0.1275	0.0941

Table 11: Comparison of our framework with some baselines.